PHYSICAL REVIEW B, VOLUME 64, 035313

Tamm-like states in finite antidot lattices

P. H. Rivera
Departamento de Física, Universidade Federal de São Carlos, 13565–905, São Carlos, São Paulo, Brazil

M. A. Andrade Neto
Curso de Ciências, Centro Universitário La Salle, Avenida Victor Barreto 2287, 92010–000, Canoas, Rio Grande do Sul, Brazil

P. A. Schulz
Instituto de Física 'Gleb Wataghin', Universidade Estadual de Campinas, 13083–970, Campinas, São Paulo, Brazil

Nelson Studart
Departamento de Física, Universidade Federal de São Carlos, 13565–905, São Carlos, São Paulo, Brazil
(Received 1 September 2000; revised manuscript received 21 December 2000; published 21 June 2001)

Transport properties of finite antidots arrays, with large lattice parameters and electron densities, may be roughly understood from a semiclassical approach. For weak magnetic fields, commensurability effects between the antidot spacing and the cyclotron radius are present with interference patterns superimposed on the magnetoresistivity. For higher magnetic fields, transport through edge states becomes relevant. In the present work, we discuss a completely different behavior that should occur in the quantum limit, for short lattice parameters and small electron densities. The key feature is the formation of surface Tamm-like states within the gap of the lowest bulk bands of a finite antidot lattice. The surface of a finite antidot superlattice may act as an isolated quantum ring, a coupler of the superlattice to the contacts, or a barrier between the bulk of the antidot lattice and the contacts, as a function solely of the applied magnetic field.

DOI: 10.1103/PhysRevB.64.035313 PACS number(s): 73.21.−b, 73.43.−f, 73.61.−r

I. INTRODUCTION

The combination of high-mobility two-dimensional electron systems (2DES's) with the possibility of patterning them down to the nanometer scale, has brought about an almost unlimited playground for research in condensed-matter physics. This statement is true from several points of view. For example, one just has to recall unexpected phenomena such as the quantum Hall effect, or a driven search for the properties of artificial atoms and molecules made of the above-mentioned low-dimensional structured semiconductor systems.

From another point of view, low-dimensional semiconductor systems modulated in so-called lateral superlattices may be considered artificial crystals, whose transport properties are tunable from a classic regime[1] to the quantum limit,[2] through a parameter range where semiclassical corrections[3] can be verified. These systems settle the context of the present work: an example of the quantum confinement effect in a mesoscopic finite crystal with unusual consequences on the electronic and transport properties of the latter. The confinement effect we are talking about is a one-dimensional analog to a Tamm state[4] in a finite antidot lattice, and the unusual properties are related to a coupling of this surface state to the bulk of the artificial crystal, that can be switched on and off by tuning a magnetic field perpendicular to the system.

Here we refer to antidot lattices as strongly modulated 2DES's, in the sense that the Fermi energy is below the potential modulation hills. Many of the transport properties of artificial crystals in the classical regime referred to above have been measured in such antidot lattices. A further enhancement of the modulation could lead to what is called a dot lattice: a Fermi sea is broken into lakes (quantum dots) and confined in the interantidot valleys, so that we have weakly interacting artificial atoms such as core states in real crystals. This transition from an antidot lattice to a dot lattice is also addressed in the present paper, concerning the robustness of the surface state effects. From the point of view of transport properties, we consider a nearly ballistic regime, i.e., a finite system where the distances between surfaces are less than the electronic mean free path.

What is usually called an infinite antidot lattice sustains a close analogy to real crystals: a mean free path larger than the crystal periodicity, but much smaller than the distance between surfaces. Since the first experimental results on magnetotransport in infinite weakly modulated lateral superlattices[5,6,2,7–13] and antidot lattices,[1,14–20] there has been a great effort from a theoretical point of view in order to shed light on the classical,[21,22] semiclassical,[23–25] or quantum[26–41] limits of these transport properties, as well as their relations to the electronic structure. On the other hand, finite square lateral superlattices[17] have received considerably less attention. In the context of the present work, one should mention the study by Zozoulenko *et al.*[34] and, very recently the work by Gudmundsson and co-workers;[40,42] the latter was related to a weakly modulated mesoscopic system and its magnetization properties.

The surface states of a finite square antidot lattice give rise to a quantum ring,[43,44] which is completely decoupled from the bulk of the system if these states are localized in a gap of the bulk-related electronic bands in the absence of a magnetic field. Turning on the magnetic field, this quantum ring couples to the bulk and decouples again at higher mag-

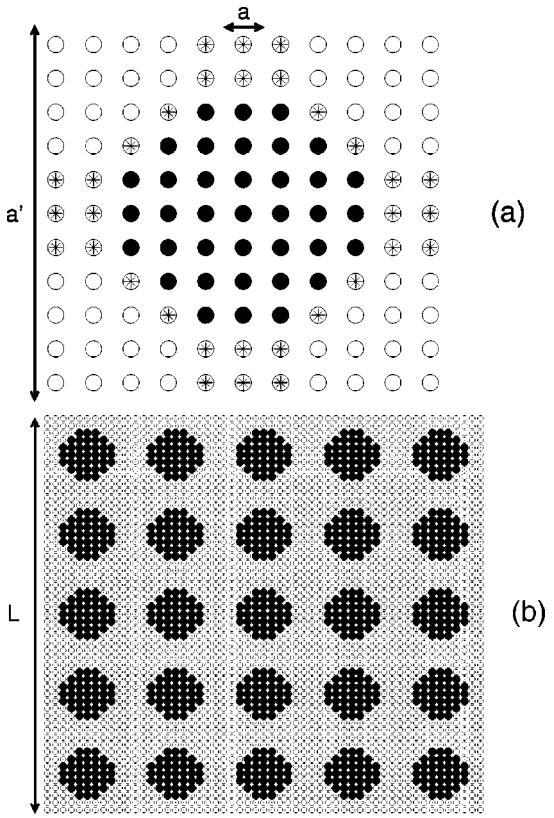

FIG. 1. (a) Antidot unit cell with a lattice parameter $a'=na$, where a is the *host lattice* constant. The color of the circles indicates the local potential profile: black for the antidot regions down to open circles for the host material. (b) Finite square 5×5 antidot array with a lateral dimension $L=ma'$ build up by repeating the unit cell shown in (a).

netic fields. By properly choosing the electronic density and the antidot spacing, the Fermi energy lies in the surface-state band, and one expects dramatic consequences in transport as a function of magnetic field, due to the one-particle electronic structure characteristics mentioned above.

The discussion of these surface state effects is the aim of the present work. We should stress the fact that these bona fide surface states are of a completely different origin than the edge states around antidots and at the edge of the confining external square reported in one of the few experimental results on such systems obtained by Schuster *et al.*[19]

The paper is organized as follows. First we briefly present the model calculation, which will be followed by a discussion of our results. We initially focus on the energy spectra of a finite lattice in the presence of a magnetic field, showing the evolution of the surface states and bulk bands as well as the spectrum change caused by going from an antidot lattice to a dotlike lattice. Next we further investigate the surface and bulklike states by means of the probability density of selected eigenvectors, as well the local current density pattern, which give further insight into the measurements of these effects by means of magnetotransport. We also discuss the influence on the spectra and current density of including wide contacts to the system in a two-terminal configuration. Finally, our results are summarized, and estimates for experimental observation of the discussed effects are given.

II. MODEL

The lower part of the energy spectrum of a two-dimensional (2D) array of antidots, that can be described in the framework of the effective-mass approximation, will be emulated here by a tight-binding model for a square lattice of *s*-like orbitals, considering only nearest-neighbor interactions.[33,34] The potential modulation is given simply by a periodic modification of the atomic site orbital energy in order to mimic a given potential profile due to the antidots. This modeling becomes clearer by referring to Fig. 1(a), where a unit cell of the square lattice showing one antidot is shown, and Fig. 1(b), where a finite array of 5×5 antidots is represented. The lattice parameter of the antidot array is $a'=na$, where a is the *host lattice* constant, and the lateral dimension of the array is $L=ma'$. The colors of the sites in Fig. 1 indicate the potential profile: black defines the antidots (barrier region), white defines the host 2D system, and gray represents an interdot potential smoothing of the small interbarrier height. The surface of the antidot array is defined by hard wall boundary conditions.

The magnetic field is introduced by means of a Peierls substitution, choosing the Landau gauge $\mathbf{A}=(0,l_1aB,0)$, leading to the following model Hamiltonian:

$$H=\sum_{l_1l_2}\{\mathcal{E}_{l_1l_2}|l_1l_2\rangle\langle l_1l_2|+V_{l_1l_2}[|l_1l_2\rangle\langle l_1+1,l_2| +|l_1+1,l_2\rangle\langle l_1l_2|]+V_{l_1l_2}e^{i2\pi\alpha l_1}[|l_1l_2\rangle\langle l_1,l_2+1| +|l_1,l_2+1\rangle\langle l_1l_2|]\}, \quad (1)$$

where l_1 and l_2 are site indexes in the x and y directions, $\mathcal{E}_{l_1l_2}=E_s$ is the atomiclike s orbital energy which is varied along the *host lattice*, and $V_{l_1l_2}$ is the nearest-neighbor hopping parameter which is kept constant to $V=-\hbar^2/2m^*a^2$ in both x and y directions.

The magnetic phase factor α is defined by $\alpha=\Phi/\Phi_e$, where $\Phi_e=h/e$ is the magnetic flux quantum, and $\Phi=a^2B$ is the magnetic flux per unit cell of the *host lattice*. Therefore, the magnetic flux through an antidot unit cell is given by $\Phi'=n^2\Phi$, and the magnetic flux through the total array is $\Phi^T=n^2m^2\Phi$.

The Schrödinger equation is solved by finding the eigenvalues and eigenvectors via standard matrix diagonalization methods. The eigenvectors are given by $|\Psi\rangle=\Sigma C_{l_1l_2}|l_1l_2\rangle=\Sigma F_{l_1l_2}$; the probability density is given by $\langle\Psi|\Psi\rangle$, and the probability current by

$$\mathbf{J}=\sum_{l_1l_2}\frac{a^2V}{i\hbar}[F^*_{l_1l_2}(F_{l_1+1,l_2}-F_{l_1-1,l_2})\mathbf{i} +F^*_{l_1l_2}(e^{-i2\pi\alpha l_1}F_{l_1,l_2+1}-e^{i2\pi\alpha l_1}F_{l_1,l_2-1})\mathbf{j}]. \quad (2)$$

III. RESULTS AND DISCUSSION

A. Parameter choice

We emulate a system with $m^* = 0.067 m_o$, using a heuristic lattice constant $a = 2$ nm, resulting in a hopping parameter $V = -142$ meV. We take the atomic *s* orbital energy for the host 2D system as $\mathcal{E}_{l_1 l_2} = 4|V| = 568$ meV, so our energy origin coincides with the bottom of the GaAs conduction band, giving an appropriate energy scale for our results.

The atomic energies for the antidotlike sites, black in Fig. 1, are shifted to $\mathcal{E}_{l_1 l_2} = 8|V|$, representing a barrier height of 568 meV. On the other hand, the atomic energies for the intermediate sites E_i (gray sites in Fig. 1) are varied between $4|V| \leqslant E_i \leqslant 4.5|V|$, representing an interdot potential smoothing around the antidots. In summary, the surface of the antidot array is modeled by an infinite barrier, while the antidots are potential barriers of ≈ 0.5 eV. All results shown here are for the structure represented in Fig. 1(b): a 5×5 array of antidots ($m = 5$) and a unit cell of 11×11 sites ($n = 11$) of the *host lattice*, with $a' = 22$ nm and $L = 110$ nm. The antidots, showing approximately a cylindrical symmetry, have an effective radius of approximately 7 nm. The lower bound is achieved when the atomic energies of the intermediate sites are $E_i = 4|V|$, while the upper bound is for $E_i = 4.5|V|$, characterizing, as will be seen in what follows, an *antidot* array and a *dot* array, respectively.

The present results are robust regarding antidot shapes and antidot lattice parameters up to $a' = 55$ nm. This has been checked for the same antidot unit cell described by an $n = 11$ array, as the results shown here, by increasing the *host lattice* parameter from $a = 2$ to 5 nm, using the same effective-mass value and consequently reducing the host band width. The choice of the finer mesh for our systematic study is a compromise between numerical costs and a good resolution of probability and local current density structures, as well as an adequate emulation of the effective-mass approximation limit.

At the end of the present work, we consider the effect of adding contacts to the closed structure of Fig. 1(b). These contacts are modeled by long strips of finite width made of the same *host lattice*, connected at the center of the left and right sides of the antidot array.

B. Energy spectra of closed antidot arrays

The starting point for describing the properties of a short-period finite-antidot array is given by the electronic structure, as a function of magnetic field, for different effective antidot radii as shown in Fig. 2. Here we focus on the very bottom of the energy spectrum, namely, the quantum limit. Recalling Sec. III A, all the spectra are for the structure depicted in Fig. 1(b) and we turn from an antidotlike system [Fig. 2(a)] to a coupled-dot array [Fig. 2(c)] by increasing the intermediate sites atomic energy only from $E_i = 4|V|$ to $E_i = 4.5|V|$. Figure 2(b) shows a transition between both limits, an antidotlike-to-dot-like lattice transition, for $E_i = 4.25|V|$. Varying the energy of these intermediate sites is the only parameter change we address in the present work. Increasing

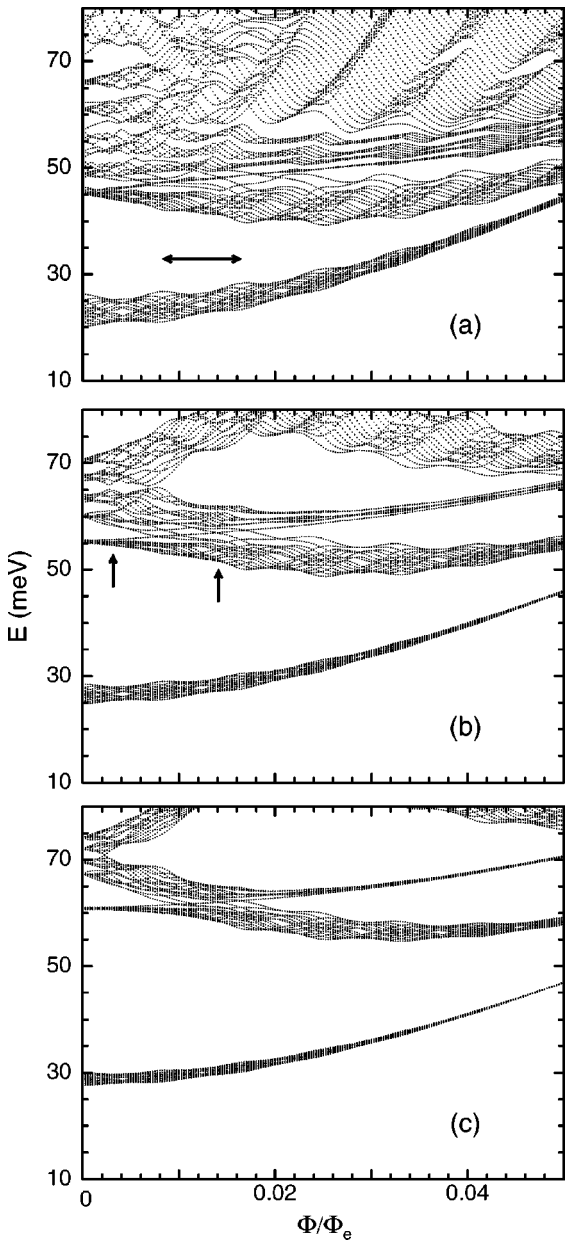

FIG. 2. Energy spectra of a 5×5 antidot lattice for three different modulation profiles as functions of magnetic field. (a) *Antidot*-like lattice. (b) *Antidotlike-to-dot* like lattice transition. (c) *Coupled-dot*-like lattice. The horizontal arrow in (a) indicates the modulation period of the incipient *core*like band. The vertical arrows in (b) are described in the text.

E_i models a saddle shape interantidot potential that could be expected, for instance, by reducing the electron density.

The lowest energy band, in all three cases, is a core bulk band, which shrinks monotonically with increasing modulation strength. For states above this core band, more dramatic changes in the spectrum occur by increasing the modulation strength. For the smallest antidot radius [Fig. 2(a)] almost a continuum of states can be seen above 50 meV. On the other hand, in Fig. 2(c) we see that this continuum of states evolves to three narrow bands. The origin of the two higher bands at zero magnetic field are the first doubly degenerate

levels of a quantum dot. This degeneracy is broken by applying a magnetic field, as expected from various previous results on isolated quantum dots.[33,45,46] One of these bands anticrosses at finite magnetic fields with a very narrow one, which is a surface state band. It can be seen in Figs. 2(a), 2(b), and 2(c) that this surface state band separates from bulklike ones with increasing potential modulation, i.e., going from an antidotlike to a dotlike finite lattice. This behavior characterizes a 1D Tamm-like state in analogy to the 2D case in finite superlattices.[4]

Signatures of an anticrossing between bulk and surface states are already seen for an antidot lattice [Fig. 2(a)] but a clearer identification of both kinds of states in the energy spectrum is obtained at a transition from an antidotlike lattice to a dotlike lattice [Fig. 2(b)]. In what follows, we will concentrate on the system described by the spectra of Fig. 2(b).

A finite array of antidots can be equivalently described as a dot lattice. The terminology is just a matter of modulation strength, as shown by the examples in Fig. 2. Therefore, the finite array of 5×5 antidots shown in Fig. 1(b) is equivalent to a 4×4 array of bulklike dots with 16 dots at the surface walls together with four ''corner dots.'' From this point of view, one can identify the bulk or surface character of the states in Fig. 2 by state counting: the first bulk core band count is 16 states, due to the ground levels of the bulk dots; while the first surface band will also have 16 states for the present case, but these will be higher in energy since the surface wall dots are smaller, splitting into groups of four states due to the presence of the corners. This can be verified by looking closer at the spectrum of Fig. 2(b) at low magnetic fields: Fig. 3(a) shows the surface state spectra in detail, and Fig. 3(b) the corelike band at low magnetic fluxes. In Fig. 3(a) we count four subbands with four states each, and in Fig. 3(b) only one band with 16 states.

Two main aspects should be emphasized as regards Fig. 3. The first one refers to the bulk band, which shows, for all cases shown in the spectra of Fig. 2, an envelope that oscillates periodically with the magnetic flux. This period, indicated by an arrow in Fig. 2(a), is approximately $\Phi/\Phi_e \cong 8\times10^{-3}$, which corresponds to a flux quantum through an antidot unit cell ($\Phi'=n^2\Phi, n=11$) in our case. This is a further signature of the bulk character of this state, and evidence that for such a small system fingerprints of bona fide bands of an infinite system are already present. Indeed, this band is a precursor of a Hofstadter spectrum:[35,41,47,48] the internal self-similar structure is not yet resolved, but a band envelope modulation scaling with an integer number of flux quantum per unit cell is clearly seen. Second, referring to the surface state band [Fig. 3(a)], the subbands also oscillate in a nearly periodic fashion. The oscillation period has an average value around $\Phi/\Phi_e \approx 7.5\times10^{-4}$, equivalent to a flux quantum through an area corresponding to the nine internal antidot unit cells, as expected if the surface state behaves as in a quantum ring.[43,44] This quantum ring behavior can be inferred from a comparison with the spectrum of an ideal one. The simplest model for a quantum ring is a one-dimensional tight-binding ring of sites, enclosing a magnetic flux, which can be treated analytically.[44] In such a simple model, the spectrum shows a particle-hole symmetry and a

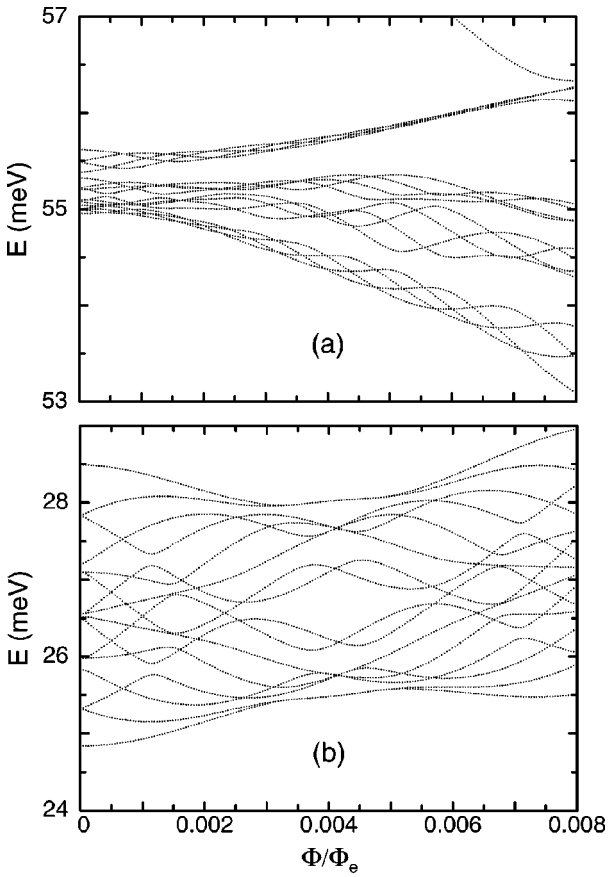

FIG. 3. Amplified energy spectra of the lowest bands in Fig. 2(b) for lower magnetic fields. (a) Surface states bands. (b) Corelike bulk band.

periodicity in the magnetic flux, with the period given by a quantum flux. The present quantum ring, a quasi-one-dimensional ring of boundary quantum dots, has a finite width and shows an internal structure in the spectrum by construction (the presence of ''corner dots,'' as discussed above). Deviations from a perfect periodicity are also expected, due to a small coupling to the second bulk band (already at very low magnetic fluxes), which is magnetic field dependent.

Having these results in mind, and considering an electronic density corresponding to a Fermi energy within the surface state band at zero magnetic field, a short-period finite antidot lattice shows an unusual behavior in this quantum limit. For very low magnetic fields the structure acts as a quantum ring. Increasing the magnetic field, the quantum ring couples to the bulk states, while a further increase of the field would make the Fermi energy lie within the second bulk band. From the point of view of transport properties, these results lead to the following inference: for low magnetic fields the structure would show persistent current effects, while, for high ones, the surface acts as a barrier between the interior of the array and eventual contacts that could be connected at the walls. These consequences on transport properties can be further characterized in what follows, where we analyze the probability densities and local current patterns related to selected states of the spectrum given in Fig. 2(b).

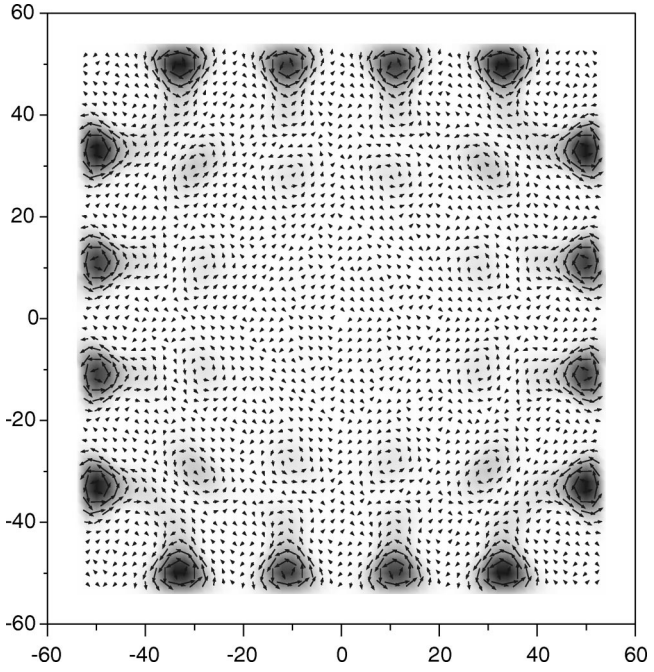

FIG. 4. Probability density and local current pattern of a surface state at $\Phi/\Phi_e = 3\times10^{-4}$.

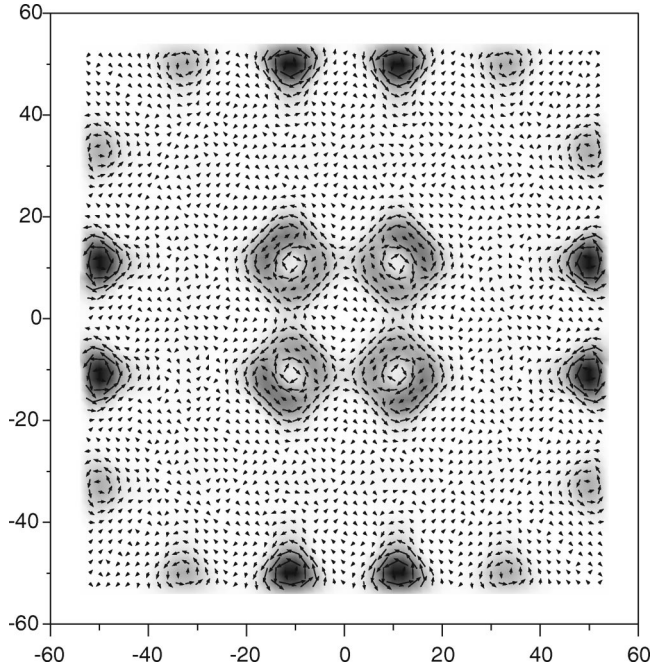

FIG. 5. Same as Fig. 4 for a coupled surface-bulk state at $\Phi/\Phi_e = 1.4\times10^{-2}$.

C. Probability and local current densities of closed arrays

A better understanding of the behavior of a finite antidot array in the quantum limit, as a function of the magnetic field, can be obtained by inspecting the probability density and local current pattern associated with individual eigenstates of the system. For the parameters chosen $\Phi = \Phi_e$, corresponds to a magnetic field $B \approx 10^3$ T. Therefore, the anticrossing in Fig. 2(b) at $\Phi/\Phi_e \approx 0.01$ corresponds to a magnetic field $B \approx 10$ T. This magnetic field value depends on the antidot spacings as well as on the modulation strength: in the case illustrated in Fig. 2(a), the anticrossing starts at $B \approx 5$ T. These are still relatively high magnetic fields, since the coupling between the bulk and the quantum ring occurring at $B = 10$ T corresponds to a magnetic length $l_B = 256/\sqrt{B} \approx 8$ nm, which is less than the interdot spacing ($a' = 22$ nm). It is important to note that the potential modulation effects are still important in the limit $l_B < a'$, as can be seen in the periodic modulation of the bulk bands of Fig. 2, as discussed above. One has to be careful to respect the limit $l_B \geqslant 2a$, below which the present approach ceases to emulate the effective-mass approximation, and the *host lattice* effects become important.

In this context, an interesting behavior related to the surface states can be observed at low magnetic fields. Figure 4 shows the probability density and local current pattern of the highest state in energy of the surface state band of Fig. 2(b) at the magnetic flux $\Phi/\Phi_e = 3\times10^{-4}$ (vertical arrow), which corresponds to $B \approx 0.3$ T and $l_B \approx 47$ nm. One can see that the probability density and the current loops are spatially squeezed at the surface at dimensions a few times smaller than the length scale given by l_B. This picture confirms the quantum ring behavior inferred from the energy spectra in Fig. 2. Due to the antidotlike potential modulation, the commensurability between the magnetic flux and the antidot spacing will determine the modulation of the probability density for the interantidot regions at the surface.

Figure 5 shows the probability density and local current pattern for a state at an anticrossing between surface and bulk states in Fig. 2(b). The magnetic flux now is $\Phi/\Phi_e = 1.4\times10^{-2}$ (vertical arrow), equivalent to a high magnetic field $B \approx 14$ T and a small magnetic length $l_B \approx 7$ nm. The coupling between bulk and surface can be clearly seen in the probability density distribution at both surface and bulk regions. The current patterns in the bulk exhibit, due to the small magnetic length, a character of edge states around the central antidots of the array, as well as hopping from one edge to the other, since the antidot effective diameter is quite large compared to the spacing between them.[11]

These probability density and local current mappings are relative to the antidot lattice whose energy spectrum is depicted in Fig. 2(b). For a weaker interdot potential modulation, as in Fig. 2(a), an edge-bulk anticrossing occurs at lower magnetic fields, for which the magnetic length is comparable to the dimension of the array itself. On the other hand, the quantum ring is less well defined, since the Tamm-like states are already merging with the bulk states at very low magnetic fields. It is important to note, however, that, in the case of Fig. 2(b), the quantum ring is well defined at low magnetic fields and the bulk band structure effects are important up to magnetic fluxes beyond the anticrossing region, as indicated by the periodic modulation of the bulk band width.

D. Contact effects

The closed systems analyzed so far fit into the context of searching fingerprints of the spectral features of Tamm-like

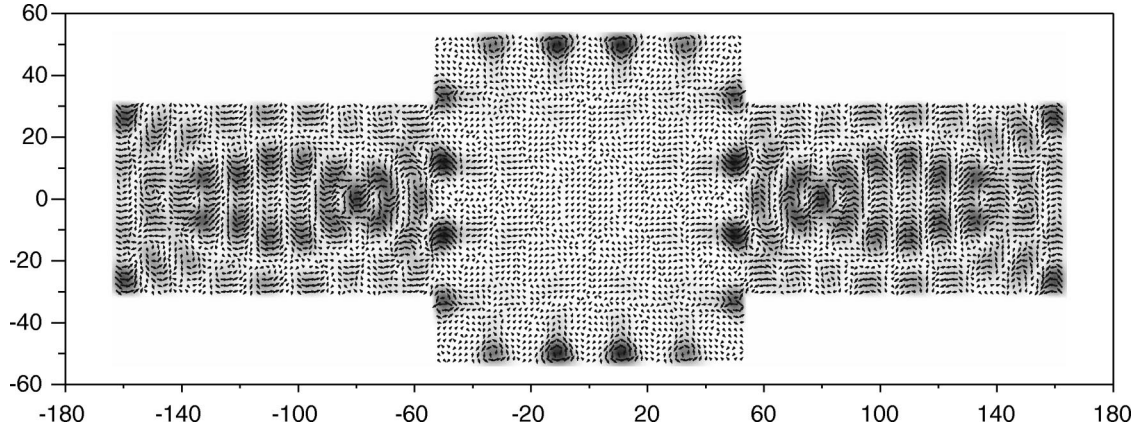

FIG. 6. Same as Fig. 4 for a Tamm state connected to contacts at $\Phi/\Phi_e = 3\times10^{-4}$.

states on the magnetization, as discussed for weakly modulated structures by Gudmundsson *et al.*[42] However, an analysis of the modifications introduced by contacts is of paramount importance regarding transport properties measurements.

For this purpose we proceed with the fundamental step of analyzing the robustness of the quantum-ring and antidot spectra fingerprints, when a continuum of states is introduced to the problem by adding contacts. We consider two contacts[34] centered at the left and right sides of the structure shown in Fig. 1(b). These contacts are finite strips, of host-material-like sites, which are quite wide (three antidot cells) and long (each contact considered is at least as long as the lateral dimension of the square array itself). These dimensions are sufficient for probing the coupling between a finite array with outer regions. The mean level separation in the surface and bulk bands of the closed structure is of the same order as in the contact regions considered; therefore, the coupling can be adequately followed as a function of either energy or magnetic flux. Furthermore, with such wide contacts, we are minimizing point-contact effects that could hinder the Tamm-like state effects. The contact regions, however, do not guarantee a bona fide continuum for calculating conductivities, for instance, a situation where infinite contacts are more appropriate. It should be mentioned that the present model is also suitable for this further step, namely incorporating infinite contacts in a similar way as in previous works.[34]

Figure 6 illustrates modifications due to the contacts on the behavior of the closed structure discussed so far: the probability density and local current pattern for a Tamm-like state coupled to contacts for $\Phi/\Phi_e = 3\times10^{-4}$ are nearly equivalent to the closed structure counterpart shown in Fig. 4. It can be seen that the quantum ring character is preserved, in spite of the wideness of the contacts. Since the magnetic length $l_B \approx 47$ nm is of the order of the strip length, strong interference effects appear in the lateral strips. It should be noted that such effects are partly present even for infinitely long strips, if l_B is of the order of the contact width. The main point here, however, is the robustness of the quantum-ring probability density and local current pattern in the presence of such contact strips. For higher magnetic fluxes these interference effects disappear, and a well-defined quantum ring now couples to edge states of the contacts (not shown here). With a further increase of the magnetic fluxes, one could see that these contact edge states first couple to the bulklike states of the array. In Fig. 7, an example of a contact-edge state coupled to the array for an energy near the anticrossing between the bulk and surface states bands of Fig. 2(b), at $\Phi/\Phi_e = 1.4\times10^{-2}$, is shown. In the unmodu-

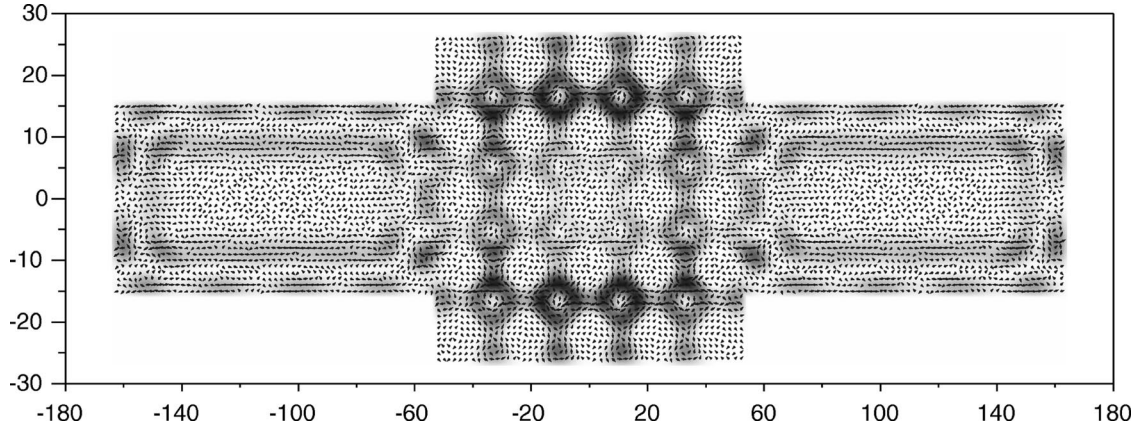

FIG. 7. Same as Fig. 4 for a coupled surface-bulk state connected to contacts at $\Phi/\Phi_e = 1.4\times10^{-2}$.

lated contacts the edge states are defined, since the magnetic length $l_B \approx 7$ nm is much smaller than the contact width (66 nm). Within the array, the probability density and local current pattern show fingerprints of a state with both bulk and surface character, like the case depicted in Fig. 5. The current pattern presents a character of internal edge states, with the edges defined by the antidots of the array, as well as interedge hopping, since, as mentioned above, the antidot effective diameter is quite large compared to the spacing between them.

IV. FINAL REMARKS

In summary, the 1D Tamm-like states of a finite square antidot lattice give rise to a quantum ring, which is completely decoupled from the bulk of the system if these states are localized in a gap of bulk-related electronic bands in the absence of a magnetic field. Turning on the magnetic field, this quantum ring couples to the bulk and decouples again at higher magnetic fields. By properly choosing the electronic density and the antidot spacing, the Fermi energy lies in the surface state band, and one expects dramatic consequences on transport as a function of magnetic field, due to the one-particle electronic structure characteristics mentioned. The surface of a finite antidot superlattice may act as an isolated quantum ring, a coupler of the superlattice to the contacts, and a barrier between the bulk of the antidot lattice and the contact, by solely increasing the magnetic field. These behaviors are the opposite of what is expected in the semiclassical limit, where the edge states at high magnetic fields only partially mimic the present surface state effects at low magnetic fields. These effects could be observable as oscillations in magnetoresistance measurements. The oscillation period should show abrupt changes as the surface states modify their role with increasing magnetic field.

Although the results shown here are for antidot periods in the range of 20–50 nm, such a length scale is still realistic considering the state of art and open possibilities of nanolithography technology. From what has been shown, the effects would be resolved by available temperatures of $T \approx 100$ mK. On the other hand, typical 2DES's with mobility $\mu \approx 100$ $m^2/V\,s$, and density $n \approx 2 \times 10^{15}$ m^{-2}, patterned in finite antidot arrays with a spacing of $a' = 40$ nm (corresponding to an effective antidot radius of approximately 14 nm, if we consider the same structure geometry of Fig. 1), would satisfy the requirements of long enough mean free paths and partially filled surface states band to warrant the observation of the above-discussed effects. On the other hand, such an electronic density in the finite array region represents a Fermi wavelength $\lambda_F \approx 56$ nm which is of the order of the typical dimensions of the system. Therefore, screening effects could be worth considering, but should not be strong enough in order to qualitatively change the phenomena pointed out here.[42]

Finally, the surface of a finite antidot array shows some peculiarities compared to the surface of a 2D superlattice.[4] Besides the difference between the surface barrier and antidot modulation heights, it is unavoidable that the dot size at the boundary is different than in the bulk of the array. This aspect is as important as the relation between barrier heights in determining the energy of the surface state band. The anticrossing between these states and the bulk state, is rather robust against the changing surface position.[49] A surface state (Tamm-like) band is nevertheless always present. For surfaces farther apart than $2a'$ from the boundary antidot centers, the quantum-ring spectrum merges into the first bulklike band,[49] which would lead to effects to be discussed in a further work.

ACKNOWLEDGMENTS

P. H. R. acknowledges the financial support of Fundação de Amparo à Pesquisa do Estado de São Paulo (FAPESP), P. A. S. and N. S. acknowledge financial support from FAPESP and CNPq.

[1] D. Weiss, M.L. Roukes, A. Menschig, P. Grambow, K. von Klitzing, and G. Weimann, Phys. Rev. Lett. **66**, 2790 (1991).
[2] T. Schlösser, K. Ensslin, J.P. Kotthaus, and M. Holland, Surf. Sci. **361/362**, 847 (1996).
[3] D. Weiss, K. Richter, A. Menschig, R. Bergmann, H. Schweizer, K. von Klitzing, and G. Weimann, Phys. Rev. Lett. **70**, 4118 (1993).
[4] I. Tamm, Phys. Z. Sowjetunion **1**, 733 (1932); H. Ohno, E.E. Mendez, J.A. Brum, J.M. Hong, F. Agulló-Rueda, L.L. Chang, and L. Esaki, Phys. Rev. Lett. **64**, 2555 (1990).
[5] D. Weiss, K. von Klitzing, K. Ploog, and G. Weimann, in *High Magnetic Fields in Semiconductor Physics II*, edited by G. Landwehr (Springer-Verlag, Heidelberg, 1989).
[6] T. Schlösser, K. Ensslin, J.P. Kotthaus, and M. Holland, Semicond. Sci. Technol. **11**, 1582 (1996).
[7] R. Schuster, K. Ensslin, J.P. Kotthaus, G. Bohm, and W. Klein, Phys. Rev. B **55**, 2237 (1997).
[8] F. Petit, L. Sfaxi, F. Lelarge, A. Cavanna, M. Hayne, and B. Etienne, Europhys. Lett. **38**, 225 (1997).
[9] S. Lüthi, T. Vancura, K. Ensslin, R. Schuster, G. Bohm, and W. Klein, Phys. Rev. B **55**, 13 088 (1997).
[10] O. Steffens, T. Schlösser, P. Rotter, K. Ensslin, M. Suhrke, J.P. Kotthaus, U. Rössler, and M. Holland, J. Phys.: Condens. Matter **10**, 3859 (1998).
[11] M. Langenbuch, R. Hennig, M. Suhrke, U. Rössler, C. Albrecht, J.H. Smet, and D. Weiss, Physica E (Amsterdam) **6**, 565 (2000).
[12] C. Albrecht, J.H. Smet, D. Weiss, K. von Klitzing, R. Hennig, M. Langenbuch, M. Suhrke, U. Rössler, V. Umansky, and H. Schweizer, Phys. Rev. Lett. **83**, 2234 (1999).
[13] B.G.L. Jager, S. Wimmer, A. Lorke, J.P. Kotthaus, W. Wegscheider, and M. Bichler, cond-mat/0005293 (unpublished).
[14] T. Yamashiro, J. Takahara, Y. Takagaki, K. Gamo, S. Namba, S. Takaoka, and K. Murase, Solid State Commun. **79**, 885 (1991).
[15] G.M. Sundaram, N.J. Bassom, R.J. Rees, P.J. Heard, P.D.

Prewett, J.E.F. Frost, G.A.C. Jones, D.C. Peacock, and D.A. Ritchie, Phys. Rev. B **47**, 7348 (1993).
[16] Y. Chen, R.J. Nicholas, G.M. Sundaram, P.J. Prewett, J.E.F. Frost, G.A.C. Jones, D.C. Peacock, and D.A. Ritchie, Phys. Rev. B **47**, 7354 (1993).
[17] R. Schuster, K. Ensslin, D. Wharam, S. Kühn, J.P. Kotthaus, G. Böhm, W. Klein, G. Tränkle, and G. Weimann, Phys. Rev. B **49**, 8510 (1994).
[18] R. Schuster, G. Ernst, K. Ensslin, M. Entin, M. Holland, G. Bohm, and W. Klein, Phys. Rev. B **50**, 8090 (1994).
[19] R. Schuster, K. Ensslin, V. Dolgopolov, J.P. Kotthaus, G. Böhm, and W. Klein, Phys. Rev. B **52**, 14 699 (1995).
[20] K. Tsukagoshi, M. Haraguchi, S. Takaoka, and K. Murase, J. Phys. Soc. Jpn. **65**, 811 (1996).
[21] C.W.J. Beenakker, Phys. Rev. Lett. **62**, 2020 (1989).
[22] W. Lu, Phys. Rev. B **54**, 8049 (1996).
[23] R. Fleischmann, T. Geisel, and R. Ketzmerick, Phys. Rev. Lett. **68**, 1367 (1992).
[24] R.R. Gerhardts, Phys. Rev. B **45**, 3449 (1992).
[25] É.M. Baskin, G.M. Gusev, Z.D. Kvon, A.G. Pogosov, and M.V. Éntin, Pis'ma Zh. Éksp. Teor. Fiz. **55**, 649 (1992) [JETP Lett. **55**, 678 (1992)].
[26] D. Pfannkuche and R.R. Gerhardts, Phys. Rev. B **46**, 12606 (1992).
[27] D. Huang and G. Gumbs, Phys. Rev. B **47**, 9597 (1993); **48**, 2835 (1993).
[28] D. Huang, G. Gumbs, and A.H. MacDonald, Phys. Rev. B **48**, 2843 (1993).
[29] J. Skjånes, E.H. Hauge, and G. Schön, Phys. Rev. B **50**, 8636 (1994).
[30] H. Silberbauer and U. Rössler, Phys. Rev. B **50**, 11 911 (1994).
[31] T. Yamuchi, Phys. Lett. A **191**, 317 (1994).
[32] S. Ishizaka, F. Nihey, K. Nakamura, J. Sone, and T. Ando, Phys. Rev. B **51**, 9881 (1995).
[33] M.A. Andrade Neto and P.A. Schulz, Phys. Rev. B **52**, 14 093 (1995).
[34] I.V. Zozoulenko, F.A. Maaø, and E.H. Hauge, Phys. Rev. B **51**, 7058 (1995); **53**, 7975 (1996); **53**, 7987 (1996); **56**, 4710 (1997).
[35] Q.W. Shi and K.Y. Szeto, Phys. Rev. B **53**, 12 990 (1996).
[36] S. Uryu and T. Ando, Phys. Rev. B **53**, 13 613 (1996).
[37] T. Nakanishi and T. Ando, Phys. Rev. B **54**, 8021 (1996).
[38] R. Neudert, P. Rotter, U. Rössler, and M. Suhrke, Phys. Rev. B **55**, 2242 (1997).
[39] T. Park and G. Gumbs, Superlattices Microstruct. **22**, 161 (1997).
[40] A. Manolescu and V. Gudmundsson, Phys. Rev. B **59**, 5426 (1999).
[41] E. Anisimovas and P. Johansson, Phys. Rev. B **60**, 7744 (1999).
[42] V. Gudmundsson, S.I. Erlingsson, and A. Manolescu, Phys. Rev. B **61**, 4835 (2000).
[43] W.C. Tan and J.C. Inkson, Phys. Rev. B **60**, 5626 (1999), and references therein.
[44] R. Kotlyar, C.A. Stafford, and S. Das Sarma, Phys. Rev. B **58**, 3989 (1998).
[45] C.S. Lent, Phys. Rev. B **43**, 4179 (1991).
[46] H. Siberbauer, J. Phys.: Condens. Matter **4**, 7355 (1992).
[47] D.R. Hofstadter, Phys. Rev. B **14**, 2239 (1976).
[48] G. Petschel and T. Geisel, Phys. Rev. Lett. **71**, 239 (1993).
[49] M. A. Andrade Neto, Ph.D Thesis, State University of Campinas, (1996).